Available online at www.sciencedirect.com
ScienceDirect
Journal of Sound and Vibration 315 (2008) 700–711
JOURNAL OF SOUND AND VIBRATION
www.elsevier.com/locate/jsvi

A study of a nonlinear vibration isolator with a quasi-zero stiffness characteristic

Ivana Kovacic[a,*], Michael J. Brennan[b], Timothy P. Waters[b]

[a]Department of Mechanics, Faculty of Technical Sciences, University of Novi Sad, 21000 Novi Sad, Serbia
[b]Institute of Sound and Vibration Research, University of Southampton, Highfield Southampton SO17 1BJ, UK

Accepted 13 December 2007
The peer review of this article was organised by the Guest Editor
Available online 30 January 2008

Abstract

A vibration isolator consisting of a vertical linear spring and two nonlinear pre-stressed oblique springs is considered in this paper. The system has both geometrical and physical nonlinearity. Firstly, a static analysis is carried out. The softening parameter leading to quasi-zero dynamic stiffness at the equilibrium position is obtained as a function of the initial geometry, pre-stress and the stiffness of the springs. The optimal combination of the system parameters is found that maximises the displacement from the equilibrium position when the prescribed stiffness is equal to that of the vertical spring alone. It also satisfies the condition that the dynamic stiffness only changes slightly in the neighbourhood of the static equilibrium position. For these values, a dynamical analysis of the isolator under asymmetric excitation is performed to quantify the undesirable effects of the nonlinearities. It includes considering the possibilities of the appearance of period-doubling bifurcation and its development into chaotic motion. For this purpose, approximate analytical methods and numerical simulations accompanied with qualitative methods including phase plane plots, Poincaré maps and Lyapunov exponents are used. Finally, the frequency at which the first period-doubling bifurcation appears is found and the effect of damping on this frequency determined.

1. Introduction

The use of passive isolators is one of the most common methods of controlling undesirable vibrations [1,2]. The performance characteristics of passive linear isolators have been widely studied [3–5]. In the simplest case when a mass m is supported by a linear spring of stiffness k on a rigid foundation, the isolator provides efficient attenuation of harmonic vibrations of frequency ω, if $\omega > \sqrt{2}\omega_0$, where $\omega_0 = \sqrt{k/m}$ is the natural frequency of the system. This indicates that the lower the static stiffness and hence natural frequency, the wider the isolation region and the more advantageous its application. However, low static stiffness causes a large static deflection. This disadvantage can be overcome by adding oblique springs in order to obtain a high static stiffness, small static displacement, small dynamic stiffness, and hence low natural frequency [2,6].

*Corresponding author. Tel.: +381 214852241; fax: +381 21458133.
E-mail addresses: ivanakov@uns.ns.ac.yu (I. Kovacic), mjb@isvr.soton.ac.uk (M.J. Brennan), tpw@isvr.soton.ac.uk (T.P. Waters).

0022-460X/$ - see front matter © 2008 Elsevier Ltd. All rights reserved.
doi:10.1016/j.jsv.2007.12.019

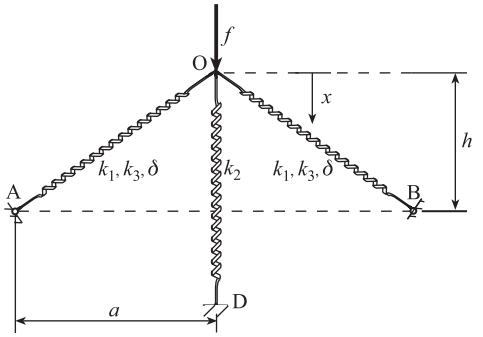

Fig. 1. A three-spring model of a QZS mechanism. The oblique springs have a cubic softening nonlinearity and pre-stress. The vertical spring is linear.

Moreover, acting as a negative stiffness, the oblique springs can yield zero dynamic stiffness, i.e. the so-called quasi-zero stiffness (QZS) mechanism can be established. This fact about the benefits of nonlinearity as well as the fact that many practical isolators exhibit nonlinear behaviour [1,7–10], has given rise to a growing interest in the study of nonlinear isolators [11–16].

In a previous study [17], a static analysis of the QZS isolator shown in Fig. 1 was presented, in which all springs were assumed to be linear and unstressed. It was concluded there that, although yielding QZS, the oblique springs detrimentally add stiffness to the vertical spring outside some displacement range and the system becomes stiffer for large excursions from the equilibrium position. The following analysis is a natural continuation of that study but with nonlinear pre-stressed oblique springs. So, unlike the previous study of a geometrically nonlinear but physically linear system, the configuration discussed in this paper is represented by both a geometrically and physically nonlinear model. The aim is to demonstrate the way in which the attachment of nonlinear oblique springs can improve the performance of a simple linear spring, and also how the introduction of physical nonlinearity in these springs can offer some benefits. The motivation is twofold. Firstly, a system configuration, which yields QZS at the equilibrium position without the detriment arising in the physically linear system is sought. Secondly, dynamic analysis of the isolator model subjected to asymmetric harmonic excitation is carried out in order to determine its behaviour.

2. Static analysis

Consider a simple model of the isolator shown in Fig. 1. Two nonlinear oblique springs are assumed to have physical nonlinearity in that they are softening, with linear stiffness k_1 and cubic softening nonlinear stiffness coefficient k_3. In addition, they are pre-stressed, i.e. compressed by length δ. These springs are connected at point O with a vertical unstressed linear spring of stiffness k_2. The geometry of the system is defined by the parameters a and h, while the coordinate x defines the displacement from the initial *unloaded* position. The relationship between the vertical applied force f and the resulting displacement x can be found by means of the principal of virtual work. This requires the total work by the force f, and the reactions of the oblique springs in the x direction f_{1x}, and the vertical spring f_2, to be zero for a virtual displacement δx, i.e.

$$(f + 2f_{1x} + f_2)\delta x \equiv 0. \tag{1}$$

The restoring force of the oblique spring f_1 is given by

$$f_1 = k_1\left(\sqrt{a^2 + (h-x)^2} - \sqrt{a^2 + h^2} - \delta\right) - k_3\left(\sqrt{a^2 + (h-x)^2} - \sqrt{a^2 + h^2} - \delta\right)^3. \tag{2}$$

Its scalar component in the x direction is

$$f_{1x} = f_1 \frac{h-x}{\sqrt{a^2 + (h-x)^2}}. \tag{3}$$

The reaction of the vertical spring is

$$f_2 = -k_2 x. \tag{4}$$

Combining Eqs. (1)–(4) gives

$$f = k_2 x + 2k_1(h-x)\left(\frac{\sqrt{a^2+h^2}+\delta}{\sqrt{a^2+(h-x)^2}} - 1\right) + 2k_3 \frac{(h-x)}{\sqrt{a^2+(h-x)^2}}\left(\sqrt{a^2+(h-x)^2} - \sqrt{a^2+h^2} - \delta\right)^3. \tag{5}$$

Introducing the dimensionless parameters

$$\hat{f} = \frac{f}{k_2\sqrt{a^2+h^2}},\quad \alpha = \frac{k_1}{k_2},\quad \hat{a} = \frac{a}{\sqrt{a^2+h^2}},\quad \hat{x} = \frac{x}{\sqrt{a^2+h^2}},\quad \hat{\delta} = \frac{\delta}{\sqrt{a^2+h^2}},\quad \beta = \frac{k_3(a^2+h^2)}{k_2}, \tag{6a–f}$$

Eq. (5) becomes

$$\hat{f} = \hat{x} + 2\alpha\Gamma(\Delta - 1) - 2\beta\Gamma P^2(\Delta - 1)^3, \tag{7}$$

where $\Gamma = \sqrt{1-\hat{a}^2} - \hat{x}$, $\Delta = (\hat{\delta}+1)/P$ and $P = \sqrt{\hat{x}^2 - 2\sqrt{1-\hat{a}^2}\,\hat{x} + 1}$.

Differentiating Eq. (7) with respect to $\hat{x}$ gives the non-dimensional stiffness of the system

$$\hat{K} = 1 + 2\alpha\left[1 - \hat{a}^2\frac{\Delta}{P^2}\right] - 2\beta(\Delta-1)^2\left[(1-\Delta)(3\Gamma^2+\hat{a}^2) + 3\Gamma^2\Delta\right]. \tag{8}$$

In operation, the system is loaded with a mass such that at the static equilibrium position ($\hat{x} = \hat{x}_e$) the oblique springs are horizontal, and $\hat{x}_e = \sqrt{1-\hat{a}^2}$. The stiffness of the system is zero provided that

$$\beta_q = \frac{\alpha}{[1-\hat{a}+\hat{\delta}]^2} - \frac{\hat{a}}{2[1-\hat{a}+\hat{\delta}]^3}, \tag{9}$$

where the subscript q denotes QZS. This relationship gives the value of the softening parameter of the oblique springs as a function of the initial geometry (parameter $\hat{a}$), pre-stress (parameter $\hat{\delta}$) and stiffness of the springs (parameter α), which leads to a QZS system. The influence of these parameters on the value of β_q is shown in Fig. 2 for different values of α. These surfaces illustrate how the optimum softening parameter of the nonlinear springs β_q is dependent on the rest of the system parameters. It should be noted that the optimum value of β_q changes profoundly depending upon the values of $\hat{a}$ and $\hat{\delta}$.

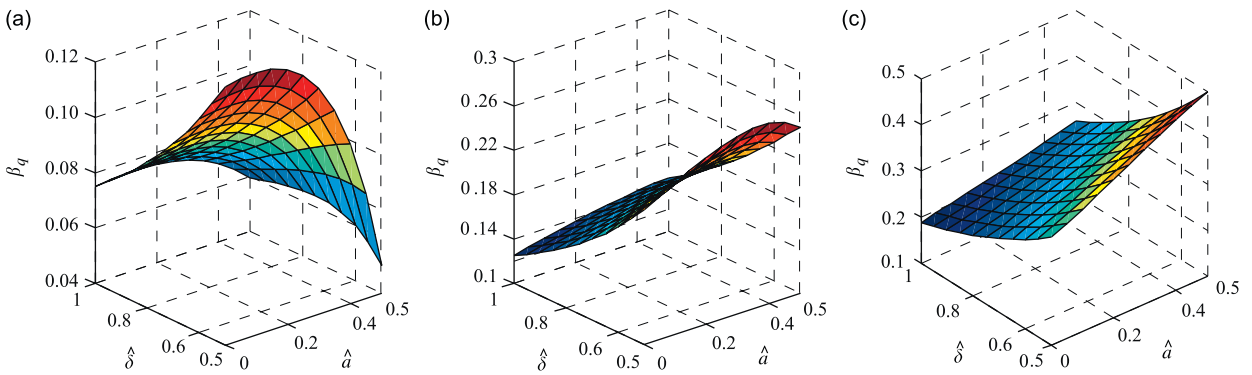

Fig. 2. The influence of the pre-stress parameter, $\hat{\delta}$, and the initial geometry parameter, $\hat{a}$, on the softening parameter of the nonlinear springs β_q for the QZS system and different values of the parameter α: (a) $\alpha = 0.3$; (b) $\alpha = 0.5$ and (c) $\alpha = 0.75$.

In the special case when the oblique springs are linear but pre-stressed, Eq. (9) reduces to

$$\hat{\delta}_q = \frac{\hat{a}(1+2\alpha)}{2\alpha} - 1. \tag{10}$$

If the oblique springs are linear and unstressed, QZS is ensured when

$$\alpha_q = \frac{\hat{a}}{2(1-\hat{a})}, \tag{11}$$

which shows that if the angle of inclination of the springs decreases, i.e. the parameter $\hat{a}$ increases, the value of α which yields QZS also increases. This result is the same as that obtained in Ref. [17].

2.1. Optimisation of the system

In addition to the isolator being a QZS system, it is desirable for it to have a wide range of non-dimensional displacements $\hat{d}$ from the static equilibrium position for which the non-dimensional stiffness is less than a prescribed low value $\hat{K}_p$. By substituting $\hat{x}_{\hat{K}=\hat{K}_p} = \hat{x}_e \pm \hat{d}$ into Eq. (8), these displacements are found to satisfy

$$\begin{aligned} &6\beta_q\hat{z}^5 - 12(\hat{\delta}+1)\beta_q\hat{z}^4 + \left[\hat{K} - 1 - 2\alpha + 6(\hat{\delta}+1)^2\beta_q - 4\hat{a}^2\beta_q\right]\hat{z}^3 + 6\gamma^2(\hat{\delta}+1)\beta_q\hat{z}^2 \\ &\quad + 2\alpha\hat{a}^2(\hat{\delta}+1) - 2\gamma^2(\hat{\delta}+1)^3\beta_q = 0, \end{aligned} \tag{12}$$

where $\hat{z}^2 = \hat{d}^2 + \hat{a}^2$.

There is no explicit analytical solution of Eq. (12). It can, however, be solved numerically, constraining various parameters. The parameters α, $\hat{a}$ and $\hat{\delta}$ are chosen from the set $\alpha \in [1/10, 10]$, $\hat{a} \in [0, 1]$ and $\hat{\delta} \in [0, 1]$. Among all the combinations of these parameters and the parameter β_q calculated using Eq. (9), only those for which the parameter β_q is positive were taken into account (only then there exists a softening spring). The optimisation criteria included the achievement of the largest displacement from the static equilibrium position, at which the prescribed stiffness was equal to that of the vertical spring alone, i.e. $\hat{K} = 1$, the condition that the stiffness should not be negative, and the requirement that the stiffness only changes slightly in the neighbourhood of the equilibrium position (the tolerance of $\Delta\hat{K} = 0.0025$ for $\Delta\hat{y} = 0.01$ was introduced, where $\hat{y} = \hat{x} - \hat{x}_e$).

The results of the optimisation are $\alpha_{\text{opt}} = 0.51$, $\hat{a}_{\text{opt}} = 0.5$ and $\hat{\delta}_{\text{opt}} = 0.89$ (for which $\beta_{q\text{opt}} = 0.1709$). These values are used to plot the stiffness of the system using Eq. (8) with respect to the coordinate system $\hat{y}$. This can be seen in Fig. 3 as the solid line, which represents the optimised system that has both geometrical and

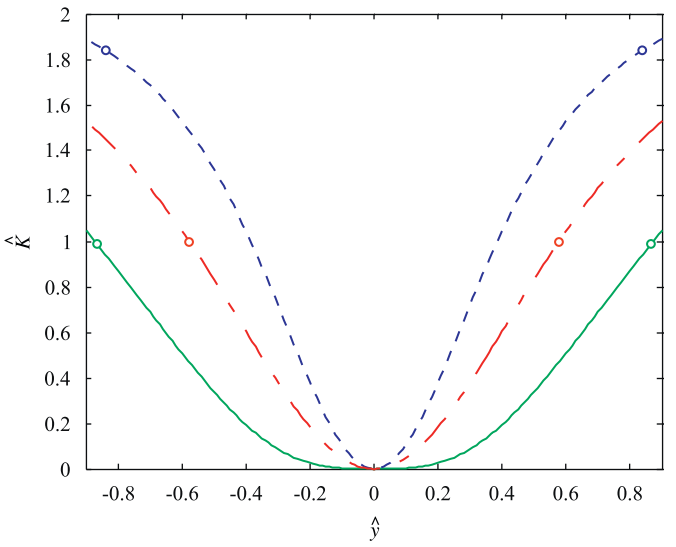

Fig. 3. Non-dimensional stiffness of the system with the linear oblique springs (dashed line), linear pre-stressed oblique springs (dashed–dotted line) and nonlinear pre-stressed springs (solid line). The circles denote the stiffness at $\hat{y} = \pm\hat{x}_e$.

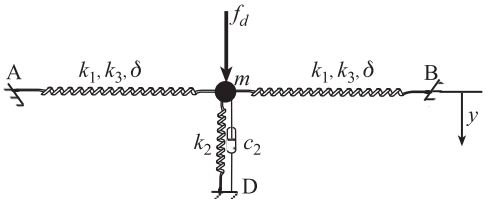

Fig. 4. Structural model of the isolator in operation.

physical nonlinearity. In addition, the results of the analytical optimisation of the linear system in Ref. [17] $\hat{a} = (2/3)^{3/2}$ and the parameter α calculated on the basis of Eq. (11) are used to plot the corresponding stiffness in Fig. 3 as a dashed line. As well as this, this stiffness is plotted in Fig. 3 for the case when the oblique springs are linear but pre-stressed with $\hat{\delta} = 0.5$ (dashed–dotted line). In this case, Eq. (10) was used as well as Eq. (12), which yields $\hat{a} = 1/\sqrt{1+\hat{\delta}}$. The circles in Fig. 3 denote the stiffness given by Eq. (8) calculated at $\hat{y} = \pm\hat{x}_e$. It can be seen that the use of nonlinear pre-stressed oblique springs can be beneficial, because it can result in a smaller stiffness for larger displacements from the static equilibrium position and, additionally, it can yield a very small stiffness in the neighbourhood of the static equilibrium position. In this way, the limitation of the linear system can be overcome and, moreover, low dynamic stiffness in the neighbourhood of the equilibrium position can be achieved.

3. Dynamic behaviour of the QZS system

When in operation, the isolator considered supports a mass m, initially in the static equilibrium position as shown in Fig. 4. To include the influence of damping, a viscous damper, with damping coefficient c_2, is added in parallel with the vertical spring. The excitation force f_d may be asymmetric, i.e. it can be the sum of a harmonic excitation $F\cos\omega t$ and a constant force corresponding to a static force F_s. Ideally, the system will only be subject to harmonic excitation about the static equilibrium position. However, in some circumstances there may be an additional "static" loading to the isolated mass due to very slowly varying inertia forces, because of the acceleration of an aircraft or vehicle in which the isolator is situated, for example.

Assuming that displacements are small, the scalar component defined by Eq. (3) in the y direction can be expanded using the Maclaurin series up to the third order. Further, taking into account the QZS condition (9), the dimensionless parameters in Eq. (6) and

$$\omega_0^2 = \frac{k_2}{m},\ \tau = \omega_0 t,\ \zeta = \frac{c_2\omega_0}{2k_2},\ \gamma = -2\beta + 3\beta\frac{1+\hat{\delta}}{\hat{a}} + \alpha\frac{1+\hat{\delta}}{\hat{a}^3} - \beta\frac{(1+\hat{\delta})^3}{\hat{a}^3},\ \Omega = \frac{\omega}{\omega_0},\ \hat{F}_s = \frac{F_s}{k_2\sqrt{a^2+h^2}}, \quad (13)$$

the non-dimensional equation of motion can be approximated by asymmetric Duffing's equation with no linear term and hardening nonlinearity

$$\ddot{\hat{y}} + 2\zeta\dot{\hat{y}} + \gamma\hat{y}^3 = \hat{F}(\cos\Omega\tau + r_f), \quad (14)$$

where

$$r_f = \frac{\hat{F}_s}{\hat{F}}. \quad (15)$$

The asymmetric Duffing oscillator has been the subject of numerous analytical and numerical investigations [18–23]. It has been shown that in this oscillator chaotic motion is preceded by a sequence of period-doubling bifurcations. In the case when the static force $\hat{F}_s$ is zero, Eq. (14) describes a symmetric Duffing oscillator. In Refs. [19,21,24,25], it has been shown that the route to or from chaos for this system is associated with the loss of stability of the third superharmonic resonant response and that this transition is a sharp one. So, in both the asymmetric and symmetric systems chaotic motion can appear, this being related to the loss of stability of the secondary resonance and the separation of two periodic solutions with different periods. The appearance of such motion in any isolation system, as in this one, is undesirable, because it can restrict its operating range

and cause irregular behaviour. The case of symmetric excitation ($r_f = 0$) is outside the scope of this paper. Thus, the following analysis is aimed at obtaining the boundaries of an operational regime of the isolator under asymmetric excitation with respect to the principal resonance curves. These boundaries are established by examining the development of period-doubling bifurcation. Approximate analytical methods and numerical simulations together with qualitative methods, such as phase plane plots, Poincaré maps and Lyapunov exponents, are used.

3.1. Approximate periodic solution, stability and bifurcation analysis

An approximate solution for the equation of motion given by Eq. (14) is found by applying the harmonic balance method. The solution is asymmetrical, comprising a bias (DC) term and harmonics (even and odd). In the region of the principal resonance, the lowest harmonic dominates, while higher harmonics are relatively small and can be omitted. Hence, the response of the system at the frequency of excitation, the so-called T-periodic solution, is assumed of the form

$$\hat{y}_0(\tau) = \hat{y}_0(\tau + T) = A_0 + A_1 \cos(\Omega\tau + \theta), \tag{16}$$

where $T = 2\pi/\Omega$, and A_0, A_1 and θ satisfy the following system of nonlinear algebraic equations:

$$\gamma A_0^3 + \frac{3}{2}\gamma A_0 A_1^2 = r_f \hat{f},$$

$$-A_1\Omega^2 + 3\gamma A_0^2 A_1 + \frac{3}{4}\gamma A_1^3 = \hat{f} \cos\theta,$$

$$-2\zeta A_1 \Omega = \hat{f} \sin\theta. \tag{17a–c}$$

The solution of this system of equations is shown in Fig. 5 in the form of the resonance curves for A_0 and A_1 for $r_f = 0.2$, $\zeta = 0.025$ and different values of the non-dimensional magnitude of the harmonic force: $\hat{F} = 0.1,\ 0.5$ and 1.

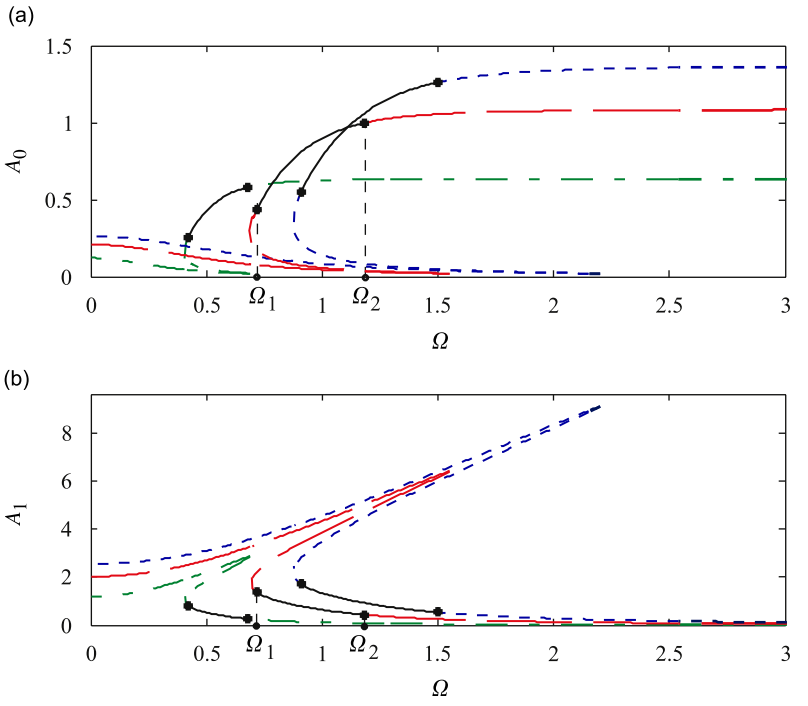

Fig. 5. (a) Resonance curves of the DC term A_0; (b) resonance curves of the harmonic term A_1 for $r_f = 0.2$, $\zeta = 0.025$ and different values of the magnitude of the harmonic excitation: $\hat{F} = 0.1$ (dashed–dotted line), $\hat{F} = 0.5$ (dashed line) and $\hat{F} = 1$ (dotted line).

In order to characterise the nature of the behaviour of the system in the neighbourhood of the solution given by Eq. (16), a perturbed solution is considered:

$$\hat{y}_1(\tau) = \hat{y}_0(\tau) + u(\tau) \tag{18}$$

for which the linear variational equation can be presented in the form of Hill's equation [26,27]:

$$\ddot{u} + 2\zeta\dot{u} + (\sigma_0 + \sigma_0 \cos\Theta + \sigma_0 2\Theta)u = 0, \tag{19}$$

where

$$\sigma_0 = 3\gamma\left(A_0^2 + \frac{A_1^2}{2}\right), \quad \sigma_1 = 6\gamma A_0 A_1, \quad \sigma_2 = \frac{3}{2}\gamma A_1^2, \quad \Theta = \Omega\tau + \theta. \tag{20}$$

It can be seen that there are two parametric excitations in Eq. (19): one with the frequency Ω and the other one with the frequency 2Ω. In a parametrically excited system, resonance occurs whenever a driving frequency is equal to $2\sqrt{\sigma_0}/n$, where n is an integer [26–28]. The first unstable region occurs for $n = 1$, i.e. close to the frequency $\Omega \approx 2\sqrt{\sigma_0}$, i.e. $\Omega \approx 2\sqrt{3\gamma\left(A_0^2 + A_1^2/2\right)}$. According to Floquet theory, the particular solution of Eq. (19) to a first approximation can be sought in the form $u(\tau) = e^{\mu\tau}v(\tau)$, where μ is the characteristic exponent and $v(\tau)$ is a periodic function with periods T and $T/2$. The solution for $u(\tau)$ is stable (respectively, unstable) if the real part of μ is negative (positive); on the boundary between stable and unstable regions the real part of μ is zero. Assuming the function $v(\tau)$ to be the first term of a Fourier series at the stability boundary $\mu = 0$, the perturbation can be written as

$$u(\tau) = b\cos\left(\frac{\Omega}{2}\tau + \phi\right). \tag{21}$$

The form of Eq. (21) indicates that bifurcation from a T-periodic solution given by Eq. (16) to a $2T$-periodic solution can appear. Inserting Eq. (21) into Eq. (19) and applying the harmonic balance method, a set of linear homogenous equations is obtained, which can be written in matrix form as

$$\begin{bmatrix} -\frac{\Omega^2}{4} + \sigma_0 + \frac{\sigma_1}{2}\cos\theta & -\zeta\Omega + \frac{\sigma_1}{2}\sin\theta \\ -\zeta\Omega - \frac{\sigma_1}{2}\sin\theta & \frac{\Omega^2}{4} - \sigma_0 + \frac{\sigma_1}{2}\cos\theta \end{bmatrix} \begin{Bmatrix} \cos\phi \\ \sin\phi \end{Bmatrix} = 0. \tag{22}$$

Non-trivial solutions exist if the determinant of the matrix in Eq. (22), denoted by D_0, vanishes

$$D_0(\Omega^2) = \left[3\gamma\left(A_0^2 + \frac{A_1^2}{2}\right) - \frac{\Omega^2}{4}\right]^2 + \zeta^2\Omega^2 - 9\gamma^2 A_0^2 A_1^2 = 0. \tag{23}$$

This determinant provides a characteristic equation for μ. Its real roots occur if $D_0(\Omega^2) < 0$ [27,29]

$$\left[3\gamma\left(A_0^2 + \frac{A_1^2}{2}\right) - \frac{\Omega^2}{4}\right]^2 + \zeta^2\Omega^2 - 9\gamma^2 A_0^2 A_1^2 < 0. \tag{24}$$

On combining Eqs. (17) and (23), the frequencies Ω_1 and Ω_2 at which period doubling occurs can be found. Using Eq. (24), a frequency region between these values can be checked to see whether or not it corresponds to instability of the T-periodic solution. However, the existence of the solutions for these frequencies will depend on the values of the parameters r_f and $\hat{F}$. This is investigated in Section 3.1.1.

3.1.1. Effects of the system parameters

In order to determine the existence of the solutions of Eqs. (17) and (23), they are solved numerically and the number of solutions is shown in Fig. 6 in the $\hat{F} - r_f$ plane for $\zeta = 0.025$, $\Delta\hat{F} = 0.01$ and $\Delta r_f = 0.01$. The case when there are two frequencies at which period doubling occurs is denoted by "o"; the case when there is no solution, i.e. period doubling does not occur is denoted by " × ". It can be seen that in the majority of cases period doubling occurs. Only when the constant force is small in comparison to the harmonic force ($r_f = 0.01$),

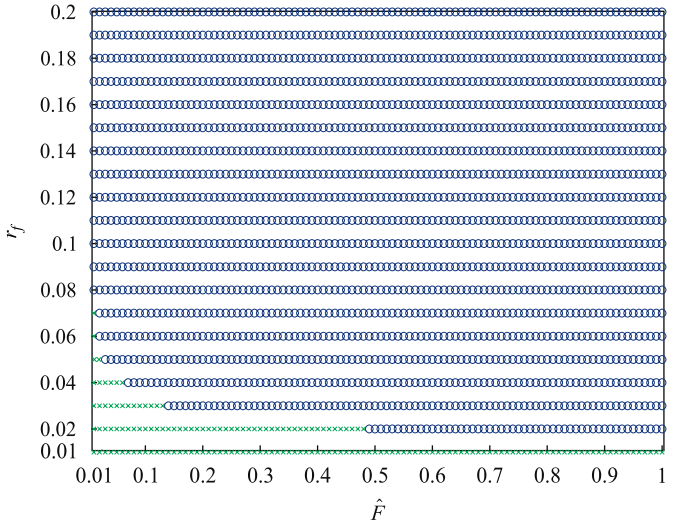

Fig. 6. The number of the values of the frequency at which period doubling occurs for $\zeta = 0.025$ as a function of the magnitude of harmonic force $\hat{F}$ and different values of the ratio r_f: "o" two values (one unstable region); " × " no values.

period doubling does not appear regardless of the value of $\hat{F}$. In addition, the smaller the magnitude of the harmonic force, period doubling does not appear for more values of the constant force.

The unstable regions are denoted in Fig. 5 with a thick black solid line. They lie on the lower non-resonant branches of $A_1(\Omega)$ and associated upper branch of $A_0(\Omega)$. The frequencies satisfying Eqs. (17) and (23) are denoted by Ω_1 and Ω_2 (for the sake of clarity they are shown just for the case $\hat{F} = 0.5$).

3.2. Numerical simulations

The analysis in the previous section shows that there is a possibility of period-doubling bifurcation and gives the system parameters at which it may occur. To verify the results of the approximate theory, numerical simulations were carried out for the equation of motion given by Eq. (14) and some selected values of the system parameters. A very fine frequency resolution to order 10^{-6} was required but the reported values are approximated to order 10^{-2}.

The bifurcation diagram corresponding to $\hat{F} = 0.5$, $r_f = 0.2$ and $\zeta = 0.025$ is plotted in Fig. 7 for decreasing frequency from $\Omega = 1.2$. It can be seen that by decreasing frequency the first period-doubling bifurcation is observed at $\Omega = 1.19$, followed by higher period doublings $4T$ at $\Omega = 1.07$ and $8T$ at $\Omega = 1.05$. This confirms the appearance of a cascade of period-doubling bifurcations 2^nT, $n = 0, 1, 2, \ldots$, developing into chaotic motion at $\Omega = 1.04$. Chaotic behaviour can also be verified by examining the Lyapunov exponents of the system (λ) [30]. For a d-dimensional dynamical system, there is a spectrum of d Lyapunov exponents. They give the rate of divergence ($\lambda < 0$) or convergence ($\lambda < 0$) of nearby trajectories in phase space. One positive Lyapunov exponent results in an exponential separation of trajectories, which corresponds to chaotic behaviour. Each type of response is characterised in the phase projections and with Poincaré maps, which are shown in Fig. 8. The sampling time for a Poincaré map was $T = 2\pi/\Omega$, so that the number of points N marked indicates the period of the response NT.

It can be seen that there is a good agreement between the value of the first period-doubling bifurcation obtained in this approach and that one found previously using Eqs. (17) and (23) with $\Omega_2 = 1.19$ (see Fig. 5a and b).

Since the system being considered is three dimensional, it has three Lyapunov exponents. When the behaviour is chaotic, they are $\lambda_1 > 0$, $\lambda_2 = 0$, $\lambda_3 < 0$ and the Lyapunov (fractal) dimension of the chaotic attractor can be estimated by [30]

$$d_f = 2 + \frac{\lambda_1}{|\lambda_3|}. \tag{25}$$

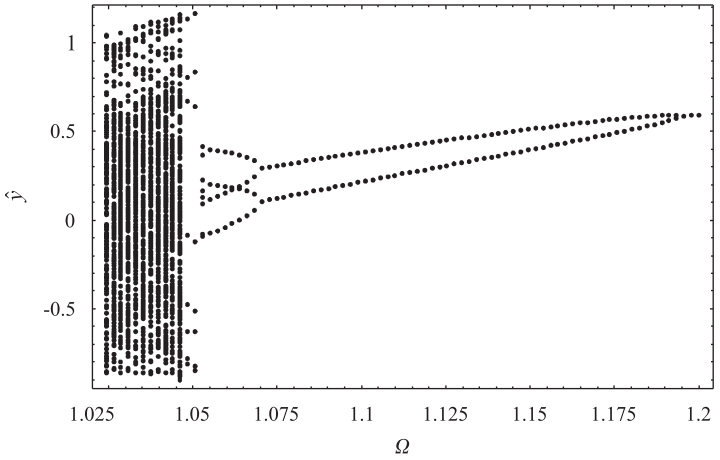

Fig. 7. Bifurcation diagram of the system for $\hat{F} = 0.5$, $r_f = 0.2$ and $\zeta = 0.025$ for decreasing frequency Ω.

When the frequency Ω decreases and passes $\Omega = 1.04$, the Lyapunov exponents are $\lambda_1 = 0.043$, $\lambda_2 = 0$, $\lambda_3 = -0.093$, which confirms the appearance of chaos. Here, the Lyapunov dimension is $d_f = 2.4624$. Not being an integer, it reveals that the system response is extremely sensitive to initial conditions.

3.3. Unstable frequency

The appearance of the first period-doubling bifurcation on decreasing frequency is of practical importance for the isolator. When the system enters the unstable region, and beyond this point chaotic motion can appear, as well as sudden and significant change of the amplitude of vibration. Hence, the first period-doubling bifurcation point can be considered as an important frequency [31,32]. Since the analysis given in the previous section has shown the accuracy of the analytical results given in Eqs. (17) and (23), they can be used to plot the graph shown in Fig. 9. This graph can be used to determine the frequency at which period doubling will emerge depending on the value of r_f and for $\hat{F} = 0.5$ (dotted line), $\hat{F} = 0.75$ (dashed–dotted line) and $\hat{F} = 1$ (dashed line).

A numerical study was carried out to determine the effect of the damping ratio on the onset of the period-doubling bifurcation point. The critical value of this parameter ζ_{cr} for which period doubling does not exist is shown in Fig. 10 as a function of the parameter r_f for different values of $\hat{F}$. It reveals that a suitable choice of the damping coefficient ($\zeta \geqslant \zeta_{cr}$) can entirely eliminate the possibility of the appearance of period-doubling bifurcation. Thus, damping can be used to suppress this behaviour of the system.

4. Conclusions

A vibration isolator consisting of a vertical linear spring and two additional springs that have both geometrical and physical nonlinearity has been considered in this paper. The additional springs are oblique, pre-stressed and have a softening characteristic. Once the system is optimised it has quasi-zero dynamic stiffness at the equilibrium position, which has been obtained as a function of the initial geometry, pre-stress and the stiffness of the springs. It has been shown that the use of nonlinear pre-stressed oblique springs can improve the static characteristics of a QZS mechanism, i.e. it can produce a smaller stiffness at larger displacements about the static equilibrium position than the system with the linear springs. Simultaneously, it can yield a very small stiffness around the equilibrium position.

However, such a nonlinear vibration isolator under an asymmetric excitation can exhibit period-doubling bifurcations. In order to characterise this behaviour with respect to the system parameters and the principal resonance, a dynamical analysis has been carried out. This analysis has led to the conclusion that in this

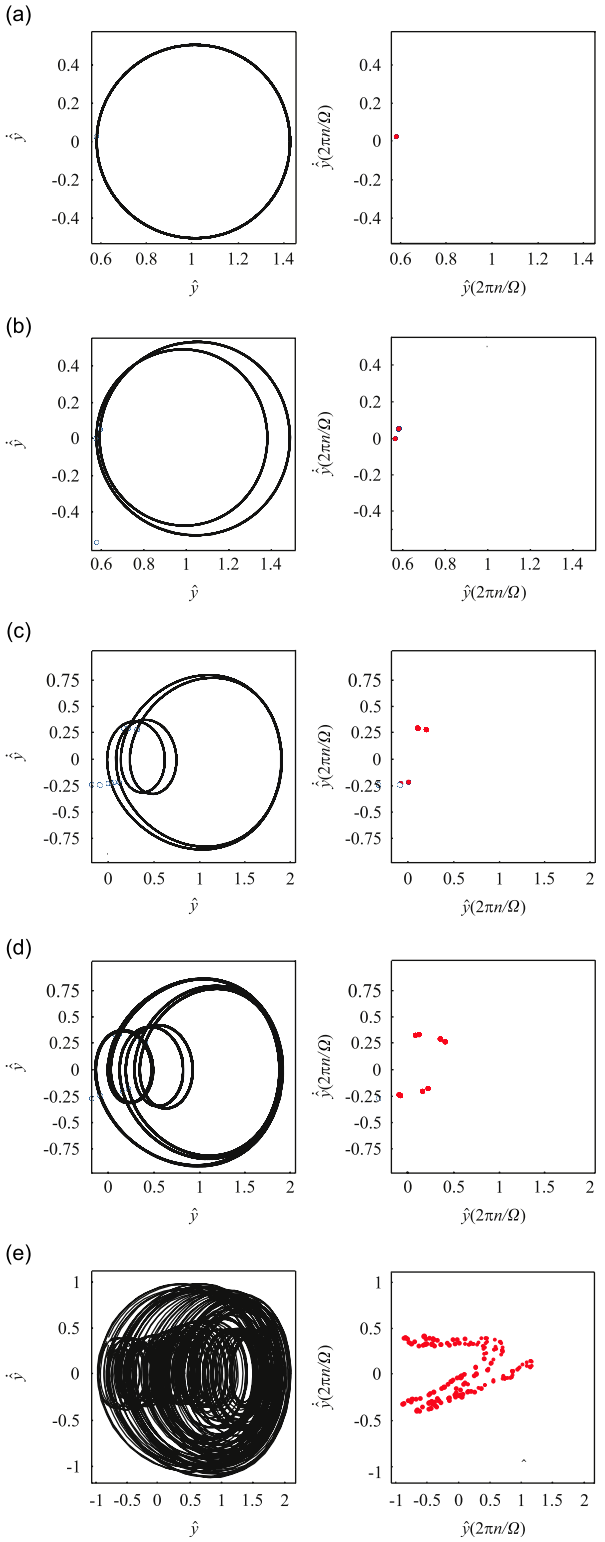

Fig. 8. Phase projections and Poincaré maps for $\hat{F} = 0.5$, $r_f = 0.2$ and $\zeta = 0.025$: (a) period-one motion $\Omega = 1.2$; (b) period-two motion $\Omega = 1.19$; (c) period-four motion $\Omega = 1.07$; (d) period-eight motion $\Omega = 1.05$ and (e) chaotic motion $\Omega = 1.04$, $\lambda_1 = 0.043$, $\lambda_2 = 0$, $\lambda_3 = -0.093$ and $d_f = 2.4624$.

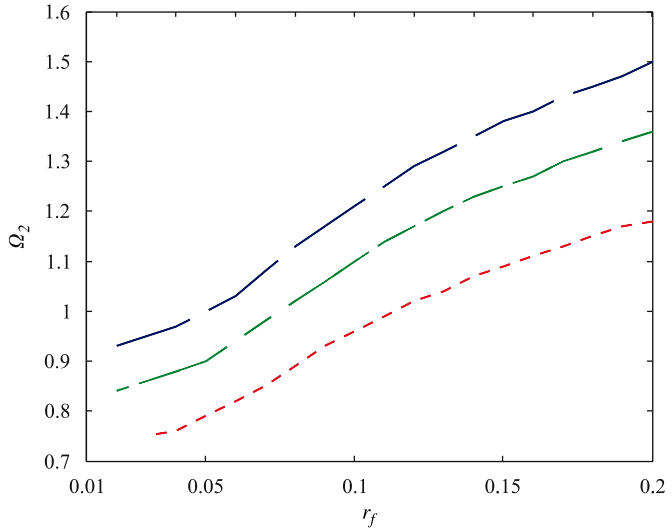

Fig. 9. The frequency at which the unstable region begins (Ω_2) as a function of the parameter r_f for $\zeta = 0.025$ and different values of the dimensionless magnitude of the harmonic excitation: $\hat{F} = 0.5$ (dotted line), $\hat{F} = 0.75$ (dashed–dotted line) and $\hat{F} = 1$ (dashed line).

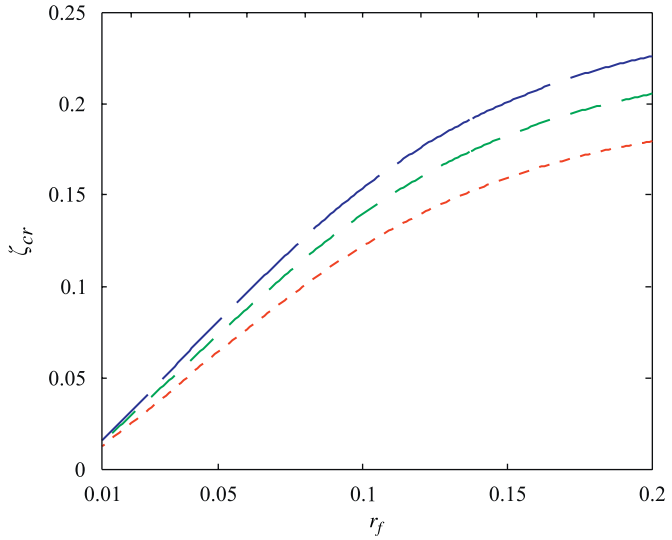

Fig. 10. The critical value of the damping ratio ζ_{cr} as a function of the parameter r_f for and different values of the dimensionless magnitude of the harmonic excitation: $\hat{F} = 0.5$ (dotted line), $\hat{F} = 0.75$ (dashed–dotted line) and $\hat{F} = 1$ (dashed line).

system period-doubling bifurcations are likely to happen within a specific frequency range. This behaviour is characterised by regions with increasing periodicity of the response, resulting in chaotic behaviour. However, for some values of the system parameters (the magnitudes of the harmonic excitation and constant forces and damping) period doubling does not occur.

Acknowledgements

This study was initiated during the stay of Ivana Kovacic at the Institute of Sound and Vibration Research, University of Southampton, United Kingdom in 2006. The stay was financially supported by the Ministry of Science and Environmental Protection, Republic of Serbia (Grant no. 451-03-00345/2006-02). The final

realisation of the study was achieved under the auspices of the Ministry of Science and Environmental Protection, Republic of Serbia (Project No. 144008).

References

[1] C.M. Harris, A.G. Piersol, *Shock and Vibration Handbook*, McGraw-Hill, New York, 2002.
[2] E.I. Rivin, *Passive Vibration Isolation*, ASME Press, New York, 2003.
[3] C.E. Crede, *Vibration and Shock Isolation*, Wiley, New York, 1995.
[4] J.P. Den Hartog, *Mechanical Vibrations*, McGraw-Hill, New York, 1962.
[5] J.C. Snowdon, Vibration isolation use and characterization, *Journal of the Acoustical Society of America* 66 (1979) 1245–1279.
[6] P. Alabudzev, A. Gritchin, L. Kim, G. Migirenko, V. Chon, P. Stepanov, *Vibration Protecting and Measuring Systems with Quasi-Zero Stiffness*, Hemisphere Publishing, New York, 1989.
[7] G. Kim, R. Singh, Non-linear analysis of automotive hydraulic engine mount, *Journal of Dynamics System, Measurement and Control—Transactions of the ASME* 115 (1993) 482–487.
[8] G. Kim, R. Singh, A study of passive and adaptive hydraulic engine mount systems with emphasis on non-linear characteristics, *Journal of Sound and Vibration* 179 (1995) 427–453.
[9] G. Popov, S. Sankar, Modelling and analysis of non-linear orifice type damping in vibration isolator, *Journal of Sound and Vibration* 183 (1995) 751–764.
[10] K. Mallik, V. Kher, M. Puri, H. Hatwal, On the modelling of non-linear elastomeric vibration isolators, *Journal of Sound and Vibration* 219 (1999) 239–253.
[11] B. Ravindra, A.K. Mallik, Performance of nonlinear vibration isolators under harmonic excitation, *Journal of Sound and Vibration* 170 (1994) 325–337.
[12] S. Natsiavas, P. Tratskas, On vibration isolation of mechanical systems with non-linear foundations, *Journal of Sound and Vibration* 194 (1996) 173–185.
[13] N. Chandra Shekhar, H. Hatwal, A.K. Mallik, Response of non-linear dissipative shock isolators, *Journal of Sound and Vibration* 214 (1998) 589–603.
[14] J.S. Tao, G.R. Liu, K.Y. Lam, Design optimization of marine engine-mount system, *Journal of Sound and Vibration* 235 (2000) 477–494.
[15] Y.P. Xiong, Y.T. Xing, W.G. Price, Interactive power flow characteristics of an integrated equipment-nonlinear isolator-travelling flexible ship excited by sea waves, *Journal of Sound and Vibration* 287 (2005) 245–276.
[16] P. Yang, J. Yang, J. Ding, Dynamic transmissibility of a complex nonlinear coupling isolator, *Tsinghua Science and Technology* 1 (2006) 538–542.
[17] A. Carrella, M.J. Brennan, T.P. Waters, Static analysis of a passive vibration isolator with quasi-zero stiffness characteristic, *Journal of Sound and Vibration* 301 (2007) 678–689.
[18] W. Szemplinska-Stupnicka, J. Bajkowski, The 1/2 subharmonic resonance and its transition to chaotic motion in a non-linear oscillator, *International Journal of Non-Linear Mechanics* 21 (1986) 401–419.
[19] W. Szemplinska-Stupnicka, Secondary resonance and approximate models of routes to chaotic motion in non-linear oscillators, *Journal of Sound and Vibration* 113 (1987) 155–172.
[20] W. Szemplinska-Stupnicka, A discussion of an analytical method for controlling chaos in Duffing's oscillator, *Journal of Sound and Vibration* 178 (1994) 276–284.
[21] B. Ravindra, A.K. Mallik, Chaotic response of a harmonically excited mass on an isolator with non-linear stiffness and damping characteristic, *Journal of Sound and Vibration* 182 (1995) 345–353.
[22] W. Szemplinska-Stupnicka, A. Zubrzycki, E. Tyrkiel, Properties of chaotic and regular boundary crisis in dissipative driven nonlinear oscillators, *Nonlinear Dynamics* 19 (1999) 19–36.
[23] J.C. Huan, Y.H. Kao, C.S. Wang, Bifurcation of structures of the Duffing oscillator with asymmetric potential well, *Physics Letters A* 136 (1999) 131–138.
[24] W. Szemplinska-Stupnicka, Bifurcations of harmonic solution leading to chaotic motion in the softening type Duffing's oscillator, *International Journal of Nonlinear Mechanics* 23 (1986) 257–277.
[25] A. Hassan, On the third superharmonic resonance in the Duffing oscillator, *Journal of Sound and Vibration* 172 (1994) 513–526.
[26] A. Nayfeh, D.T. Mook, *Nonlinear Oscillations*, Wiley, New York, 1979.
[27] C. Hayashi, *Nonlinear Oscillations in Physical Systems*, McGraw-Hill, New York, 1964.
[28] J. Kevorkian, J.D. Cole, *Perturbation Methods in Applied Mathematics*, Springer, New York, 1981.
[29] A. Hassan, On the local stability analysis of the approximate harmonic balance solution, *Nonlinear Dynamics* 10 (1996) 105–133.
[30] A. Wolf, J.B. Swift, H.L. Swinney, J.A. Vastano, Determining Lyapunov exponents from a time-series, *Physica D* 16 (1985) 285–317.
[31] A.A. Al-Qaisia, M.N. Hamdan, Bifurcations of approximate harmonic balance solutions and transition to chaos in an oscillator with inertial and elastic symmetric nonlinearities, *Journal of Sound and Vibration* 244 (2001) 453–479.
[32] S.-C. Chang, H.-P. Lin, Non-linear dynamics and chaos control for an electromagnetic system, *Journal of Sound and Vibration* 279 (2005) 327–344.